Photoactivity of Titanium Dioxide Supported on MCM41, Zeolite X, and Zeolite Y

Yiming Xu and Cooper H. Langford*

A110, University of Calgary, Calgary, Alberta T2N 1N4, Canada

Received: August 14, 1996; In Final Form: January 26, 1997[⊗]

Titanium dioxide supported on microporous zeolites of type X and Y and on mesoporous molecular sieves of the MCM41 type was studied for the photocatalytic degradation of acetophenone in an aqueous medium. The photoactivity of the supported catalyst is strongly influenced by the method of titania loading, but less affected by the temperature at which the sample was calcined. The highest photoactivity among the supported catalysts is observed for a support that has a lower Si/Al ratio in the framework and relatively large pore size. The measured apparent activation energies for photocatalyzed consumption of acetophenone for a commercial TiO_2 (P-25) and 10 wt % TiO_2-loaded samples of zeolite A, X, Y, and Al-MCM41 are 4.2−6.7, 16.9, 13.5, 32.2 and 3.6 kJ/mol, respectively. Selective doping by Fe, Mn, and V into the framework of MCM41 suppresses the photoactivity of the supported titanium dioxide. The physical state of the titanium dioxide on the supports is characterized by XRD, adsorption and pore size analysis, IR, and Raman spectroscopy. All methods emphasize the small particle or amorphous character of the TiO_2. The normal phase transition to rutile does not occur at higher temperatures on zeolite supports. In some cases, very low loadings of TiO_2 appear to achieve total absorption of the light entering the reaction vessel. For the Al-rich MCM41-supported catalysts, maximal photoactivity can be achieved at low TiO_2 loading (<3%). It appears to absorb 100% of light entering the reaction vessel with a much lower TiO_2 load than is the case with TiO_2 itself. There is evidence that the crystallinity of the zeolite is an important factor in photocatalytic efficiency, but the mechanism of zeolite participation in reactions remains incompletely elucidated.

Introduction

TiO_2 particles have been utilized to promote the photocatalytic degradation of various organic compounds.[1,2] The photocatalytic efficiency of TiO_2 is greatly influenced by crystal structure, particle size, surface area, and porosity, as determined by different preparation methods.[3−6] Increasing the photocatalyst surface area is the most obvious means of improving the efficiency of photocatalytic oxidation reactions.[3] Practical application[1] requires these fine TiO_2 particles of high surface area to be fixed on an inert support so that the recovery from the treated effluent is simplified. The fixation of titanium dioxide onto a glass matrix,[7] optical fibers,[8] and a stainless-steel plate[9] has been studied. Unfortunately, the photocatalytic efficiency of immobilized TiO_2 is often lower than the suspended TiO_2 particles. An alternative route for supporting fine TiO_2 particles on porous materials of larger particle size has been investigated using silica gel,[10] active carbon,[11] sand,[12] clay,[13,14] and zeolite.[15−19] These studies have included an effort to increase the adsorption of organic substrates on the catalyst surface for improving the efficiency of photocatalytic oxidation.[19]

Among various supports for TiO_2 photocatalysts, zeolites seem attractive candidates.[15−19] The well-defined porous structures of zeolites may offer a special environment for fine titania particles, possibly with unusual morphologies and thus altered photoactivity. It has been reported that titanium dioxides encapsulated inside zeolite Y through ion-exchange[15,16] or pillared into the interlayers of clays[14] do not have either anatase or rutile crystalline structure, but are photoactive toward the photocatalytic oxidation of organic compounds in aqueous media. We have recently observed[19] that for the photodegradation of acetophenone or 4-chlorophenol in an aqueous medium supported titania on a hydrophobic molecular sieve, ZSM5, shows high photoactivity even at low Ti loading. In this sample, the Ti−O vibrations are significantly perturbed by linkages to the support. The same report notes that the photoactivity of supported titania on zeolite A is affected by crystallinity of zeolite in the sample. Some questions raised include the possibility of zeolite structure enhancement of TiO_2 activity,[19] the possibility of zeolite effect on stability of reactive species such as hydroxyl radicals or intermediates, and the possibility of adsorption on zeolite enhancing delivery of organic substrates to TiO_2 sites.[20,21]

To begin to address some of these questions, we have selected a variety of supports for TiO_2 photocatalysts including the microporous zeolites of type X and Y with varying Si/Al ratio and the mesoporous MCM41 family with varying pore size, Si/Al ratio, and crystallinity. Zeolites X and Y have topologically similar aluminosilicate framework structure with a pore diameter of about 0.74 nm,[22] but the supercage in zeolite X (Si/Al ratio = 1.4) is more polar than in zeolite Y (Si/Al = 2.4).[23,24] MCM41 possesses regular one-dimensional channels with mesopore diameters ranging from 1.6 to 10 nm.[25] Ultrafine TiO_2 particles (called Q-sized) in the nanometer range[26] can penetrate the pores of the support. High-silica zeolite Y is the unique support in this set to examine the effect of variable zeolite hydrophobicity (as Si/Al ratio is varied) on the photoactivity of supported titania.

The physical state of the titanium dioxide on/in the support is examined by powder X-ray diffraction (XRD), Raman spectroscopy, adsorption, and pore size analysis. Photoactivity of the catalyst is evaluated using the photocatalytic oxidation of acetophenone as the test reaction. We have also investigated the effect of transition metal ions (Fe, Mn, Ti, V), substituted into the framework of MCM41 on the photoactivity of supported TiO_2, and the effect of varying experimental parameters such as titania loading methods, calcining temperature, and pH of the aqueous medium. Finally, the activation energy for photocatalyzed conversion of acetophenone is measured for a series of representative photocatalysts.

[⊗] Abstract published in *Advance ACS Abstracts,* March 15, 1997.

S1089-5647(96)02494-7 CCC: $14.00

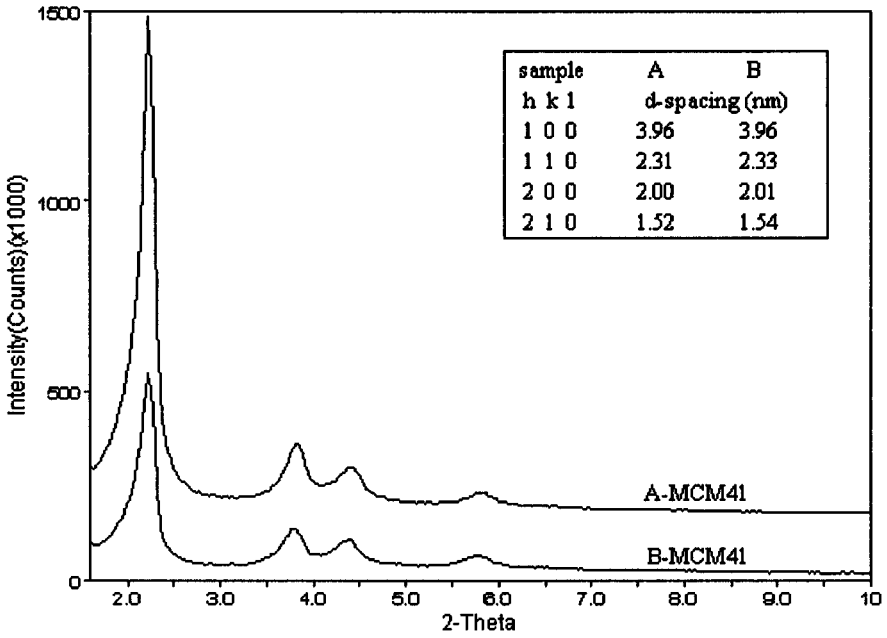

Figure 1. X-ray powder diffraction patterns of A-MCM41 and B-MCM41 samples.

Experimental Section

Materials. Titanium tetraisopropoxide (97%), acetophenone (99%), zeolites of type X and Y in the sodium form, cetyltrimethylammonium (CTA) chloride (25 wt % aqueous solution), and dodecyltrimethylammonium (DTA) bromide were purchased from Aldrich. P25 TiO_2 and zeolite Y samples with high Si/Al ratios of 28, 55, and 100 were kindly provided by Degussa Corp. Silica (Ludox HS40, 39.5 wt % SiO_2) and sodium aluminate (Anachemia) were used as received.

Synthesis of MCM41. The procedures used for the synthesis of siliceous MCM41 (type A, B, or C) and aluminosilicate MCM41 (Al-MCM41) were similar to those presented by Breck et al.[25] with some modifications. A template solution of CTA or DTA hydroxide was prepared by the exchange of CTA-Cl or DTA-Br (25 wt % aqueous solution) with aqueous ammonia (28 wt %).[27] Ludox HS40 (39.5 wt % SiO_2) and sodium aluminate were used as the source of silica and alumina, respectively. Surfactant DTABr was used only for C-MCM41 synthesis. The molar composition of final gel mixtures was $6SiO_2$:CTACl or DTABr:$1.5Na_2O$:$0.15NH_3 \cdot H_2O$:$250H_2O$, and for Al-MCM41 the Si/Al ratio was adjusted to 30. The reaction mixture was loaded into a polypropylene bottle and heated without stirring at 90−95 °C for 3 days (2 days only for B-MCM41).[28] The solid product was filtered, washed with 4 L of distilled water, and dried in air at 100 °C overnight. The solid was finally calcined directly in air at 540 °C for 10 h (heated from room temperature to 540 °C with a heating rate of 1 °C/min). The structure and quality of final materials were confirmed by both XRD and adsorption isotherms, consistent with those reported by Beck et al.[25] Figure 1 shows the XRD patterns of A-MCM41 and B-MCM41, and Figure 2 shows the nitrogen adsorption isotherms for the final solids of A-MCM41, C-MCM41, Al-MCM41, and titania-loaded Al-MCM41, respectively. Structural parameters are collected in Table 1.

Various substituted MCM41 (with Ti,[29] Fe,[30] Mn,[31] and V,[32]) were prepared according to the methods of the cited reference. Surfactant CTACl was always used as the template. The metal salts used in the syntheses were $Mn(NO_3)_2$ (Alfa, 99.98%), $Fe(NO_3)_3$ (BDH, 98.0%), $VOSO_4$ (Pfaltz & Bauer), and titanium(IV) tetraisopropoxide, respectively. The molar ratio of Si/M (Ti, Fe, Mn, and V) in the final gel mixture was 24 for Ti-MCM41, 40 for Fe-MCM41, 23 for V-MCM41 and 20 for Mn-MCM41. The final calcined solids showed the relatively well-defined XRD diffraction patterns, typical of MCM41 as presented in Figure 1. The *d*-spacing of the (100) plane was 39.5 Å for Mn-MCM41, 36.8 Å for Fe-MCM41, and 38.2 Å for V-MCM41. An exception was Ti-MCM41, where the XRD pattern was poorly resolved and showed only a strong peak from

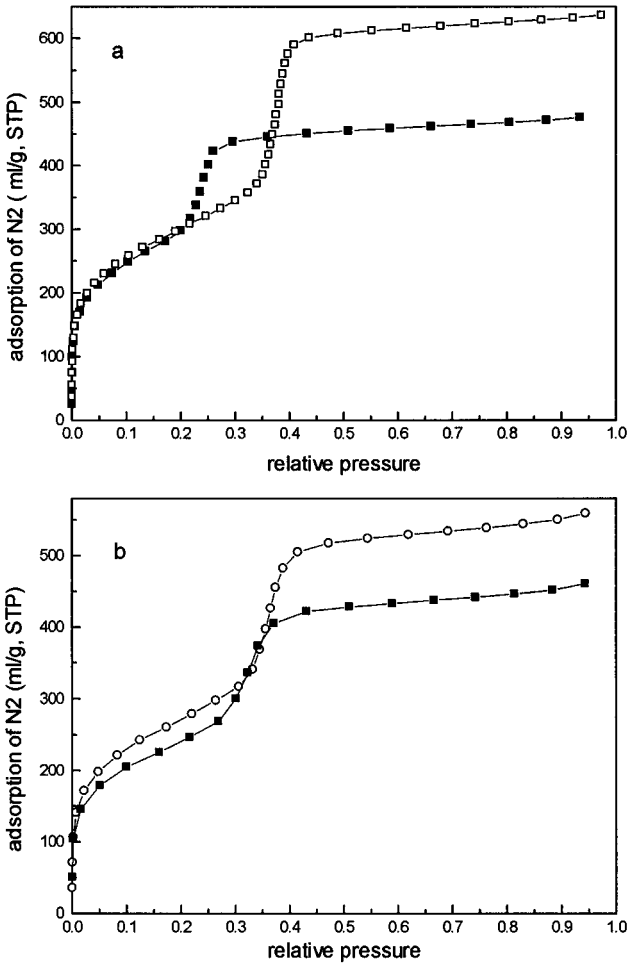

Figure 2. Adsorption isotherms of nitrogen on different MCM41 samples: (a) A-MCM41 (□); C-MCM41 (■); (b) Al-MCM41 (○), 10 wt % TiO_2/Al-MCM41 (■).

TABLE 1: Structure Parameters of Synthesized MCM41 Obtained from XRD Analysis and Nitrogen Adsorption at −196 °C

samples	d_{100} (Å) spacing	BET (m^2/g)	V_{ad}[a] (mL/g STP)	V_p (mL/g)[b]	pore size (Å)[c]
A-MCM41	39.6	1105	630	0.975	35.7
B-MCM41	39.6	1109	639	0.988	35.2
C-MCM41	33.3	1093	474	0.733	25.7
Al-MCM41	38.0	985	555	0.858	34.8

[a] Pore volume from adsorption of N_2 at $P/P_0 = 0.9$. [b] Pore volume calculated by Gurvitsch rule. [c] Pore diameter calculated by using the Horvath−Kawazoe model.

a d_{100} of 35.0 Å, similar to those presented in the reference.[29] The IR spectra of substituted MCM41s show a shoulder at 961−969 cm^{-1}, indicative of the incorporation of metal ions into the framework of molecular sieves.

Preparation of Photocatalysts. The supported TiO_2 photocatalysts were prepared by two different methods. Method A was used by us previously.[19] The sample was prepared by slurrying a titania sol (denoted AT) with the powder form of the supports. Subsequently the dried solid was calcined at 450 °C. The TiO_2 sol (AT) was synthesized by the hydrolysis of titanium isopropoxide in the presence of ethanol and nitric acid, and then the mixture was refluxed for 8 h. The particle size of the AT sol is larger than the pore size of any of the supports. Method B was essentially the same as method A, but using a titania sol (denoted QT) where the particle size is about 2−4 nm,[26] much smaller than those of AT sol, as evidenced by the cloudy look of AT sol while QT sol is transparent. The QT sol was prepared by the controlled hydrolysis of titanium isopropoxide in the presence of ethanol and nitric acid at 4 °C and maintained at 4 °C for 10 h with vigorous stirring.[26] Then 1.5 g of support powder was added to 100 or 200 mL of QT sol, and the mixture was stored in an ice-bath for 3 days with occasional shaking. The solvent was removed from the final suspension by a rotary evaporation at 35 °C. The dried solid was heated in an oven overnight and calcined at 450 °C for 11−12 h. The samples prepared by method A or method B are named as AT-"support" or QT-"support" in this text. As an example, the label AT/X represents AT-loaded zeolite X.

The catalysts designed for the purpose of calcination temperature studies were prepared by method A. Zeolite X or Y was loaded by AT-titania at 10 wt % (calculated). Before calcination, the powder (dried initially at 110 °C) was divided equally into eight samples. Each of them was then calcined at different temperature from 150 to 730 °C for 11−12 h. Elemental analysis showed that there was only 0.61 wt % of carbon present even in a parallel-prepared pure AT-TiO_2, which was calcined at a lowest temperature of 150 °C. This indicates that the hydrolysis of titanium isopropoxide is quite complete.

In this report, Ti content in the catalyst is reported as TiO_2 wt %, calculated from the amount of titanium added into the support during its synthesis. It was confirmed early[19] that the measured content of TiO_2 in samples was close to that calculated from synthetic conditions, as expected.

Characterization. Powder XRD diffraction data were collected on a Scintag XDS 2000 X-ray diffractometer using Cu Kα radiation. IR spectra were recorded on a 4030 Galaxy Series Mattson FTIR instrument using self-supported KBr pellet techniques. A typical pellet contains about 1 wt % sample in KBr. Raman spectra were collected on a Jarrel-Ash Model 25-100 spectrometer.[19] UV−vis absorption spectra were measured on a Hewlett-Packard HP 8452 diode array spectrophotometer.

Nitrogen adsorption isotherms were measured at −196 °C using an ASDI RXM-400 apparatus. Prior to the experiments, samples were degassed at 250 °C for at least 3 h until a pressure of 10^{-7} Torr was obtained. During the isotherm measurement, data were collected when the pressure changed at a rate smaller than 0.02 Torr/min. The volume of adsorbed N_2 was normalized to standard temperature and pressure (STP). The pore size distribution was calculated from the adsorption branches of the N_2 adsorption isotherm using the method of Horvath and Kawazoe,[33] as suggested by Beck et al.[25]

Acetophenone Adsorption in the Dark. The relative adsorption capacities of some of the supported titania photocatalysts for organic substrate were evaluated in aqueous media. A 50.0 mL sample of aqueous acetophenone solution of various initial concentrations was mixed with 0.250 g of the catalyst. This suspension was shaken at 20 ± 2 °C in the dark for more than 12 h, so as to reach the equilibrium (the decrease of acetophenone concentration in the bulk was not obvious even after the mixture was shaken for 1 h). The mixture was then filtered through a Millipore filter (0.45 μm pore diameter). The concentration of acetophenone in the filtrate was determined by standard GC technique on a Hewlett-Packard Model 5880 GC instrument operating with a flame ionization detector and a capillary column (DB-24, 15 m long and 0.32 mm in diameter, J & W Chromatograghies) run at an oven temperature of 130 °C. For the high-silica zeolite Y samples, where adsorption was substantial, an adsorption constant and capacity were then calculated assuming applicability of the Langmuir equation.

Photoactivity Measurements. The relative photocatalytic activities of various catalysts were evaluated by measuring the loss of acetophenone from the aqueous phase as a representative reaction. The procedure was the same as previously reported.[19] The irradiation source was a 200 W xenon lamp with a 350 nm cutoff filter. A sample of 0.50 g of catalyst and 100 mL of acetophenone solution with a typical concentration of 50 ppm were mixed in the glass reactor. The reactor was stirred constantly at a temperature of 20 ± 2 °C. The suspension was air-saturated before sealing, and oxygen was not deliberately purged into the reactor during the experiment. Prior to commencing irradiation, the suspension was typically equilibrated for 2 h, except in the case of higher organic adsorption, where the stirring time was extended to more than 12 h to assure the dark equilibrium. Total irradiation time was 2 h for each sample in the comparison runs. Small aliquots of the suspension were withdrawn by syringe, filtered through a Millipore filter membrane, and analyzed by GC. The photodegradation process of acetophenone tends to follow pseudo-first-order kinetics, and the data were fitted to the corresponding logarithmic expression to get an apparent rate constant k in min^{-1}. This rate constant is not regarded as fully interpretable since we know that a complete kinetic treatment includes substrate concentration dependence varying from zero to first order and variable dependence on light intensity.[2c] The first-order rate constants under a fixed condition serve to compare relative activity of catalysts.

Results and Discussion

1. Photoactivity of Zeolite X and Y Based Catalysts. Zeolite X (Si/Al = 1.4) shows a higher supported TiO_2 photoactivity than zeolite Y (Si/Al = 2.4). Figure 3 shows how the catalyst photoactivity varies with titania loading. In both cases, the apparent rate constant, k, increases with TiO_2 loading, approaching a limit at 20−25 wt % of TiO_2. This limit corresponds to about 1 g/L of TiO_2, similar to the value found for zeolite A as a support and found for unsupported TiO_2 as well.[19] This indicates that the quantity of TiO_2 required to adsorb all the photons entering the reactor is essentially the same as in the absence of support. The limiting rate constant of AT/X is about 1.4 times that shown by AT/Y. The supported titania

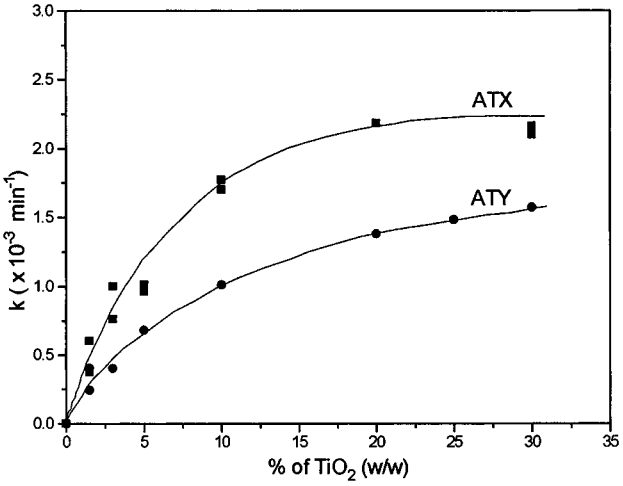

Figure 3. Photoactivity changes for the photodegradation of acetophenone by TiO_2/zeolte X (■) and TiO_2/zeolite Y (●) with Ti loading.

TABLE 2: Apparent Rate Constant of Acetophenone Photodegradation in the Presence of TiO_2 at Different pH[a]

sample	initial pH at 6	initial pH at 10
unsupported TiO_2	6.9×10^{-4}	9.6×10^{-4}
Degusa P25 TiO_2	2.2×10^{-3}	3.5×10^{-3}

[a] Initial concentration of acetophenone is 53 ppm, and catalyst 2.0 g/L.

has higher limiting photoactivity then unsupported AT-TiO_2 prepared in parallel (Table 2), but is not superior to a good commercial TiO_2 such as Degussa P-25. In this case, adsorption onto the catalyst surface is not a factor responsible for the difference in photoactivity, since acetophenone has a similar dark adsorption on these two catalysts (5.0% of initial 50 ppm at the catalyst concentration of 5.0 g/L).

As noted in Table 2, the TiO_2-catalyzed photodegradation of acetophenone is pH-dependent, and the degradation is faster in a basic medium. In this case, the aqueous suspensions of zeolite X and Y (5 g/L) give a pH of 10.0 and 8.5, respectively. The zeolite effect on pH is a significant factor in the small observed difference in photoactivity between the AT/X and AT/Y catalysts.

Slightly different morphology of supported titania on X and Y can be seen in XRD patterns. In both cases, the reflection at $2\theta = 25.3°$, characteristic of anatase, increases with titania loading. The XRD peak at half-height is wider on zeolite X than on zeolite Y. Assuming width is determined by particle size, the particle sizes of anatase "crystallites" on zeolite X and Y at a coverage 30 wt % TiO_2 are aboutg 4.6 and 6.5 nm, respectively, as estimated using the Scherre equation.[34] Unsupported TiO_2 (AT) prepared in parallel has an apparent particle size of 24 nm. The Raman spectra of these samples correspond reasonably to anatase titanium dioxide.

All these results emphasize the role of the supports in influencing the reactivity and morphology of the supported TiO_2 and extend the conclusion of our earlier paper.[19]

2. Effect of Calcining Temperature. Several parallel samples of the zeolite-supported titania, calcined at temperatures from 150 to 730 °C, were studied. Figure 4 presents the photoactivities of 10 wt % TiO_2-loaded zeolite X and Y as a function of calcination temperature. The photoactivity of the supported titania on zeolite X decreases somewhat with the increase of temperature, while the activity of the supported titania on zeolite Y shows little change over the wide range of calcination temperature. Several authors[35] have reported that the photoactivity of pure TiO_2, prepared by a method similar to that used in this paper, is greatly effected by the sintering

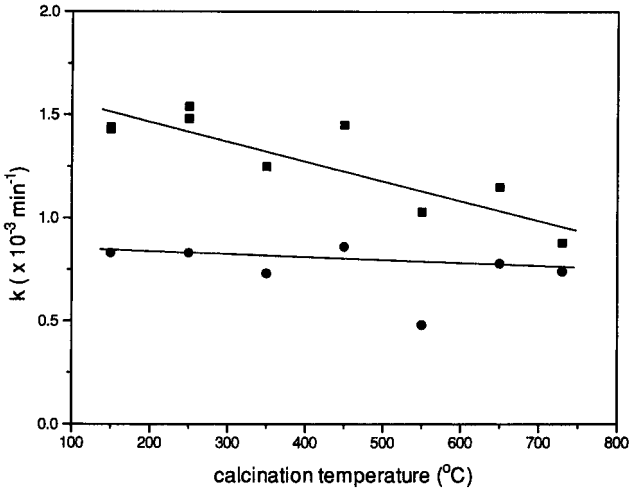

Figure 4. Photoactivities of AT/X (■) and AT/Y (●) with 10 wt % of TiO_2 loading as a function of calcination temperature.

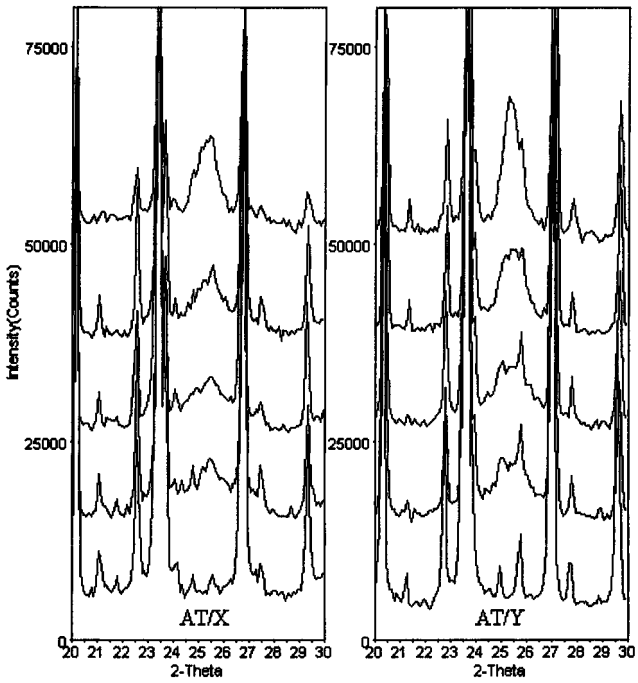

Figure 5. X-ray powder diffraction patterns of AT/X and AT/Y with 10 wt % of TiO_2 loading as a function of calcination temperature. The pattern from bottom to top corresponds to the sample of bare zeolite and ATX or ATY calcined at 250, 450, 650, and 730 °C, respectively.

temperature, increasing with temperature up to 400 °C[35a] in one case or 550 °C in others,[35c,d] then decreasing dramatically above this temperature. Our results suggest that TiO_2 supported on zeolites has somewhat higher activity in small particle (or even amorphous) forms at low temperature.

The XRD patterns of these samples are shown in Figure 5. Supported titania does not show the expected phase transformation from anatase to rutile even at 730 °C. On both the supports, reflection at the anatase angle of 25.3° is seen from 150 °C. This is in agreement with Raman spectra. The TiO_2 reflections sharpen with increase of temperature. This suggests particle growth with increasing temperature, but quite little, as compared to unsupported TiO_2. Up to 730 °C, the apparent size of supported titania particles is not larger than 10 nm. Unsupported TiO_2 particles appear to grow from 8 to 32 nm up to 550 °C in the anatase form and then grow to 47 nm at 730 °C in the rutile form with the phase transition between 450 and 550 °C. Zeolites prevent the fine titania particles from both sintering and phase transition upon calcination. This supported titania

TABLE 3: Physical Parameters of the Titania-Loaded MCM41, Characterized by XRD and Nitrogen Adsorption at −196 °C[a]

sample	d_{100} (Å)	BET (m^2/g) meas	BET (m^2/g) calc	V_p (cm^3/g) meas	V_p (cm^3/g) calc	ΔV_p[b]	pore size (Å)[c]
QT/A-MCM41	39.1	955	992	0.837	0.877	−0.040	35.0
QT/B-MCM41	39.2	982	998	0.844	0.889	−0.045	35.2
QT/C-MCM41	31.9	956	984	0.642	0.660	−0.018	25.4
QT/A1-MCM41	36.3	882	887	0.707	0.772	−0.065	32.3
AT/A-MCM41	39.0	994	992	0.843	0.877	−0.034	34.8
AT/C-MCM41	32.2	947	984	0.646	0.660	−0.014	25.3

[a] 10 wt % of TiO_2 content in all the samples; QT as well as AT represents the origin of titania sols. See the Experimental Section for the details. [b] ΔV_p represents the difference between the measured (meas) and calculated (calc) pore volume. $V_p(\text{calc}) = 0.90\mathbf{V_p}$ where $\mathbf{V_p}$ is the pore volume, listed in Table 1, of the corresponding pure MCM41. [c] Pore diameter.

on a nearly constant scale of several nanometers has nearly constant photoactivity (Figure 4).

3. TiO_2 Supported on the Mesoporous Molecular Sieves of MCM41. To evaluate the titanium dioxide located in the pores of the mesoporous zeolites, mesoporous molecular sieves of MCM41 materials[25,29−32] were studied as a support for TiO_2. The MCM41 supports used in this study include pure siliceous MCM41s with different pore size and crystallinity and the framework-incorporated MCM41 samples containing Al, Fe, Mn, Ti, and V. These supports have high surface areas of over 950 m^2/g and large pore sizes ranging from 2.57 to 3.57 nm in diameter (Table 1). These pore sizes exceed TiO_2 colloidal particle size in the case of QT-TiO_2 sols, where the particle size is about 2−4 nm.[26] We will see below that titanium dioxide can be incorporated into the pores of MCM41. AT-TiO_2 particles cannot enter pores.

Characterization. Figure 2b shows the adsorption isotherm of nitrogen on 10 wt % TiO_2-loaded Al-MCM41. Pore volumes are decreased by TiO_2 loading even if we assume that TiO_2 itself has a zero pore volume and deduct the weight of TiO_2 from the total weight of the sample prior to comparison. Table 3 summarizes the data, together with d_{100} spacings from XRD. As can be seen in the table, the pore volume decreases in all the cases by an amount from 0.014 to 0.065 mL/g after correction for 10 wt % of TiO_2. Comparing data in Table 1, we see that the pore diameter and d_{100} spacing are decreased by titania loading especially in the case of QT-loaded Al-MCM41, where d_{100} spacing and pore diameter change by about 1.7 Å. These results suggest partial incorporation of titanium dioxide into MCM41 pores. If titania exists in the form of anatase with a density of 3.79 g/cm^3, 10 wt % of TiO_2 would occupy a volume of 0.0263 mL/g of the supported sample. Volume decreases range up to −0.065 mL/g, suggesting that effective densities of supported TiO_2 are lower or TiO_2 blocks access to some pores. We favor that latter interpretation.

XRD of the samples, loaded by the two different TiO_2 sols, larger (AT) and smaller (QT) particles, shows no obvious difference in the diffraction patterns (not presented in this text). Reduced relative titania intensity of Al-MCM41 may imply that there is more titania in the interior mesopores, consistent with the result from pore volume analysis.

Photoactivity of MCM41-Based Catalysts. The method of titania loading has major impact on the photoactivity. Surprisingly, all QT-loaded samples showed little measurable photoactivity in the standard acetophenone test, whereas the corresponding AT-loaded samples are photoactive. For the pure TiO_2 prepared in parallel, QT-TiO_2 is also less photoactive than the AT-TiO_2, probably because of more defect sites associated with QT-TiO_2 that is prepared at lower temperature by sol-gel techniques.[5b] Our results suggest that during the loading process the MCM41 supports offer a porous environment for incorporating the nanosized titania particles.

Table 4 lists the rate constants for the samples of AT-loaded siliceous MCM41 as well as the fraction of acetophenone adsorbed in the dark prior to illumination. The rate constants for supported titania on A-MCM41 are usually higher than those for supported titania on B-MCM41. These two supports are siliceous MCM41 and have the same pore size (Table 1). The aqueous suspension of both supports gives a pH of 4.5. The obvious difference between these two molecular sieves is the crystallinity. A-MCM41 has substantially greater crystallinity compared to B-MCM41, as evidenced by the peak intensity of d_{100} diffraction shown in Figure 1. The results here support our early zeolite A observation[19] that the photoactivity of the supported titania is correlated with the crystallinity of the support. This effect is not well understood, but we suspect that the electric field, provided by the zeolite framework, and the mobilities of the adsorbed/dissolved oxygen species may be important.

The pore size of the mesoporous support has no obvious effect on the photoactivity of AT-loaded materials. (We will show elsewhere, using energy-filtered TEM, that the particles retain the size of the initial colloid and are not in equilibrium, during the loading, with smaller TiO_2 fragments which might enter the pores.) As shown in Table 4, the rate constants of supported titania of C-MCM41 (2.57 nm) may be slightly smaller than those on A-MCM41 (3.57 nm), but larger than those on B-MCM41 (3.52 nm). If crystallinity is considered, the d_{100} diffraction intensity of C-MCM41 is between those of A-MCM41 and B-MCM41 supports. Lack of a clear pore size effect suggests that the diffusion of reactive species along the mesoscale channels is sufficient for the photooxidation of acetophenone, since it is clear that acetophenone can enter channels. As will be shown below, the activation energy for MCM41-supported catalyst is the smallest among all the photocatalysts studied, which supports the hypothesis of facile diffusion.

Titania (AT) supported on Al-substituted MCM41 produces the highest photoactivity observed among the MCM41 supports. Figure 6 shows the photoactivity as a function of Ti loading. As with the ZSM5 support,[19] the photocatalytic efficiency is high even at a coverage of 3 wt % of TiO_2, having a rate constant of 1.5×10^{-3} min^{-1}. This suggests again that the light adsorption is efficient in a thin film of titanium dioxide and that the adsorbed acetophenone on the surface can efficiently reach these light-activated sites. The higher activity than siliceous MCM41 may relate to greater pore size reduction by TiO_2 loading. The suspension of Al-MCM41 gives a solution pH of 4.8. Adsorption of acetophenone in the dark prior to illumination amounted to 10−13% under the same conditions as used for Table 4 runs. At all TiO_2 loading, the lower adsorption capacity of Al-MCM41 is no doubt due to lower hydrophobicity than siliceous MCM41.[27]

An effort to affect photoactivity by doping transition metal ions into the framework of MCM41 support was made. Titania loaded on the supports of Fe-, Mn-, and V-MCM41 shows no measurable photoactivity. The color of the solids is brown-yellow for Fe-MCM41, brown for Mn-MCM41, yellow for V-MCM41, and white for Ti-MCM41 (which is active), respectively. The lack of the photoactivity is the result of inner filter effects of transition metal light absorption in these supports. The colorless Ti-MCM41 loaded with titanium dioxide has a photoactivity similar to silicous-MCM41 (Table 4), but Ti-MCM41 itself is not photoactive under the present conditions.

4. Titania Supported on a High-Silica Zeolite Y. Preconcentration of organic substrates on the catalyst surface may

TABLE 4: Apparent Rate Constants, k ($\times 10^{-3}$ min^{-1}), for the Samples of AT-TiO_2-Loaded MCM41

sample	(%TiO_2)	ad (%)[a]	k	sample	(%TiO_2)	ad (%)[a]	k
A-MCM41	10	24	0.65 ± 0.06	C-MCM41	10	25	0.73 ± 0.09
	20	16	1.4 ± 0.12		20	24	1.3 ± 0.05
	40	14	1.4 ± 0.15		40	17	1.2 ± 0.12
B-MCM41	10	19	0.68 ± 0.09	Ti-MCM41	10	20	0.84 ± 0.13
	20	18	1.0 ± 0.07	Ti-MCM41	20	18	1.2 ± 0.09
	40	10	0.9 ± 0.15		40	15	1.4 ± 0.02

[a] The dark adsorption percentage of acetophenone on the catalyst prior to illumination. conditions: initial AP concentration of 50 ppm and catalyst concentration of 5 g/L. Dark equilibrium time of overnight.

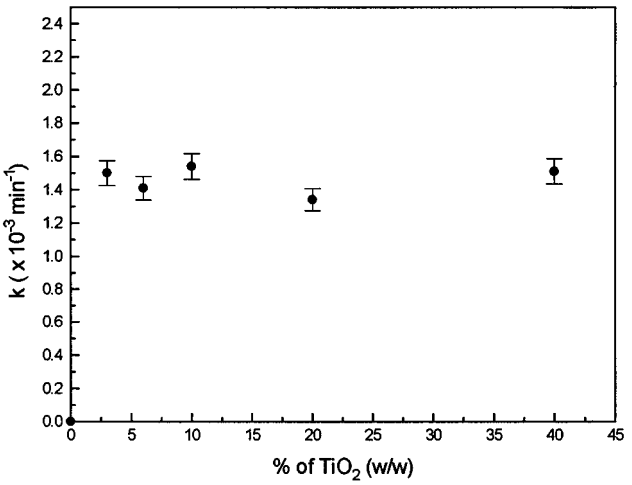

Figure 6. Photoactivity of AT/Al-MCM41 as a function of TiO_2 loading for the photodegradation of aqueous acetophenone.

TABLE 5: Langmuir Adsorption Parametres for the Acetophenoe Adsorption on High-Silica Zeolite Y Loaded by TiO_2 from an Aqueous Media

	n_{max} (mmol/g)			K (L/mmol)		
TiO_2% (w/w)	Si/Al = 28	Si/Al = 55	Si/Al = 100	Si/Al = 28	Si/Al = 55	Si/Al = 100
0	1.79	1.81	2.03	5.4	9.0	18
14	1.50	1.40	1.69	5.1	8.5	10
24	1.37	1.22	1.37	3.4	3.8	14

enhance the interfacial reactions of the adsorbed substrate with the photogenerated reactive species by reducing diffusion to a two-dimensional process. Such preconcentration may be achieved by using a more hydrophobic zeolite as the support of the TiO_2 photocatalyst. Several high-silica zeolite Y samples with variable ratio of framework Si/Al were studied to see the effect of the Si/Al ratio on the substrate adsorption and thereafter on the photoactivity with a zeolite crystal structure identical to normal high-alumina zeolite Y.

Unlike the alumina-rich zeolite Y with a Si/Al ratio of 2.4, the high-silica zeolite Y samples strongly adsorb acetophenone from aqueous media. To make a quantitative comparison, adsorption isotherms were measured initially. The experiments were carried out in the dark by shaking aqueous acetophenone solutions with the catalyst at a constant temperature for more than 12 h. The isotherm thus obtained fits the Langmuir equation well.[36] Two parameters K and n_{max}, a measure of adsorption intensity and capacity, respectively, were evaluated. Table 5 summarizes results obtained for all the titania-loaded and bare samples. Both the adsorption K value and adsorption capacity (n_{max}) become larger as the Si/Al increases. K and n_{max} both decrease with the Ti loading. Capacity (n_{max}) decreases somewhat more than the reduction in wt % of zeolite Y in the total sample weight.

The adsorbed acetophenone is located in the micropores of the zeolite. This is indicated by the magnitude of the calculated zeolite void volume from the maximum adsorption of acetophenone (n_{max}, Table 5). The calculated void volume of the parent zeolite Y varies from 0.256 to 0.211 cm^3/g as the Si/Al ratio from 2.5 to 49 in NaY[37] (estimated by vapor adsorption of benzene). Using the Si/Al ratios of 28, 55, and 100, let us assume that all the porous spaces are filled only by acetophenone molecules and the density of the adsorbed acetophenone is the same as in the liquid (1.03 g/cm^3); this leads to pore volumes of 0.209, 0.219, and 0.237 cm^3/g, respectively. These values agree qualitatively with the literature data for benzene. The similarity of the values demonstrate uptake of acetophenone within zeolite Y pores. As the Si/Al ratio increases, unit cell size shrinks, and the void volume measured by benzene decreases. In aqueous media, however, water uptake into the zeolite pores occurs. The opposite order shown by the acetophenone adsorption implies higher water content inside the zeolite pores of zeolite Y with a lower Si/Al ratio. The adsorbed acetophenone competes with the adsorbed water.

Photoactivity of TiO_2 supported on these high-silica zeolite Y materials was disappointing. In tests, the suspension was pre-equilibrated overnight before the initiation of illumination. The concentration of acetophenone in bulk phase decreases only in the initial 15 min of irradiation, after which changes are quite slow. This kind of "self-deactivation" was found for all the TiO_2-loaded zeolite Y with a high Si/Al ratio, but was not observed with the Al-rich zeolite Y, having a Si/Al ratio of 2.4. There is certainly a similarity (difficult to quantify) in initial slopes for some high Si/Al ratio samples and normal (Si/Al = 2.4) zeolite Y.

Several additional experiments were conducted to explore the reactivity of the adsorbed acetophenone. An aqueous suspension of acetophenone and 24 wt % TiO_2-loaded zeolite Y (Si/Al ratio of 24) was irradiated continuously for 4 h. This suspension was then extracted with chloroform to recover acetophenone. No substantial decrease in the total quantity of acetophenone was found, and the mass balance was satisfactory. In another separate experiment, the acetophenone-loaded solid was collected from the suspension before and after irradiation. IR analysis of solid pellets indicates that there is no loss in the total content of C═O and also no shifts in the C═O vibrational band at 1686 cm^{-1}. An increase in oxygen concentration in the suspension (presaturation by dioxygen) also failed to enhance the substrate photodegradation. Reactive species generated from the irradiated TiO_2, located mostly on the external surface of the support, may be inaccessible to the acetophenone substrate adsorbed inside the support pores. However, the inhibition of loss from the bulk after a short period argues against a distinct surface reaction. All the experiments performed so far suggest that the photoactivity toward acetophenone of the supported titania on the high-silica Y is quite low.

5. Activation Energy. Apparent activation energy is an important parameter. If the reaction rate depends simply on the rate of generation of the e^-/h^+ pairs, the activation energy (E_a) will be zero. For the reactions of various organic substrates, however, the measured apparent E_a has been reported in the range 0−17 kJ/mol.[38] The apparent E_a for the photodisappearance of 4-chlorophenol depends on the concentration of oxygen

TABLE 6: Activation Energy, E_a, for the Commercial TiO_2 and for the 10 wt % TiO_2-Loaded Zeolites and Al-MCM41

sample	E_a (kJ/mol)	sample	E_a (kJ/mol)
TiO_2 P25, pH 6	4.2 ± 1.9	TiO_2/zeolite X	13.5 ± 0.4
TiO_2 P25, pH 11	6.4 ± 1.9	TiO_2/zeolite Y	32.2 ± 2.3
TiO_2 MCB, pH 6	6.7 ± 4.2	TiO_2/Al-MCM41	3.6 ± 1.7
TiO_2/zeolite A	16.9 ± 0.7		

and of the organic substrate.[38] This suggests bimolecular processes involving oxidant and reductant molecular species.

A series of apparent rate constants for acetophenone loss were measured as a function of temperature over the range 20−60 °C for each catalyst. Arrhenius plots yield E_a values that are summarized in Table 6. Two samples of commercial TiO_2 at an initial pH of 6 and 11 and four samples of the supported TiO_2 with 10 wt % of TiO_2 content (Al-MCM41, zeolite Y with a Si/Al ratio of 2.4, zeolite X, and zeolite A) were examined. The apparent E_a differs significantly among the supported TiO_2 catalysts. The order of E_a values by support is zeolite Y > zeolite A > zeolite X > no support > Al-MCM41. The initial pH (6 or 11) and the origin of TiO_2 have little influence on the value of E_a in the case of a commercial TiO_2 as the catalyst. Sources of a difference in E_a include the step of trapping the photogenerated electrons or holes by oxygen, water, substrate, or by the oxide matrix, temperature dependence of sorption of O_2 and acetophenone, and the step of the diffusion of reactive species such as surface holes, $^{\bullet}OH$, oxygen radicals, and acetophenone molecules. In the cases of the supported titania, the large differences in E_a are probably related to differences in the mobility and the diffusion of reactive species. Since the support is critical, the difference in surface diffusion of acetophenone is a leading candidate for explanation of the differences observed.

Conclusion

The results of the present survey underline the considerable variation in photoactivity of similar TiO_2 phases (the AT-TiO_2-derived samples) when they are supported on various zeolites. In all cases, however, the zeolite support prevents growth of large TiO_2 crystallites and prevents conversion to the rutile phase. The XRD data suggest that TiO_2 remains in small particles or perhaps in an amorphous form related to anatase. It is notable that the zeolites do not appear to scatter photons in ways that prevent efficient absorption of light by TiO_2. We see cases where significantly smaller weights of TiO_2 correspond to the light absorption limit than is the case with unsupported TiO_2 alone. Some results support an earlier observation that the crystal structure of the zeolite can be critical. Some of the supported photocatalysts are quite promising, but controlling factors remain incompletely elucidated.

Acknowledgment. This work was sponsored by a strategic grant from the Natural Science and Engineering Research Council of Canada. We thank the Degussa Corp for their generous gifts of the high-silica zeolite Y and P-25 TiO_2. We thank Prof. R. Kydd for his helpful discussions and for the use of his laboratory facilities in the synthesis of MCM41 materials and adsorption and Raman spectra measurements. Help from Dr. A. Starosud is also acknowledged.

References and Notes

(1) (a) Ollis, D. F., Al-Ekabi, H., Eds. *Photocatalytic Purification and Treatment of Water and Air*; Elsevire Science Publishers B. V: Amsterdam, 1993. (b) Helz, G. R., Zepp, R. G., Crosby, D. G., Eds. *Aquatic and Surface Photochemistry*; Lewis Publishers: Boca Raton, FL, 1994; Part II.

(2) (a) Pelizzetti, E., Schiavello, M., Eds. *Photochemical Conversion and Storage of Solar Energy*; Kluwer Academic Publishers: Dordrecht, 1991. (b) Serpone, N., Pelizzetti, E., Eds. *Photocatalysis-Fundamentals and Applications*; Wiley Interscience: New York, 1989. (c) Mattews, R. W. In ref 2a, p 437.

(3) Dagan, G.; Tomkiewicz, M. *J. Phys. Chem.* **1993**, *97*, 12651. Pichat, P., Guillard, C.; Almalric, L.; D'Oliveira, J.-C. In ref 1a, p 207.

(4) Hoffmann, M. R.; Martin, S. T.; Choi, W.; Bahnemann, D. W. *Chem. Rev.* **1995**, *95*, 69.

(5) (a) Sclafani, A.; Palmisano, L.; Schiavello, M. *J. Phys. Chem.* **1990**, *94*, 829. (b) Martin, S. T.; Herrmann, H.; Choi, W.; Hoffmann, M. R. *J. Chem. Soc., Faraday Trans.* **1994**, *90*, 3315.

(6) Serpone, N.; Lawless, D.; Khairutdinov, R. *J. Phys. Chem.* **1995**, *99*, 16655.

(7) Serpone, N.; Borgarello, E.; Harris, R.; Cahill, P.; Borgarello, M. *Sol. Energy Mater.* **1986**, *14*, 121. Chester, G.; Anderson, M. A.; Read, H.; Esplugas, S. *J. Photochem. Photobiol. A: Chem.* **1993**, *71*, 291. Xu, Y.; Chen, X. *Chem. Ind. (London)* **1990**, *6*, 497. Vinodgopal, K.; Hotchandani, S.; Kamat, P. V. *J. Phys. Chem.* **1993**, *97*, 9040.

(8) Hofstadler, K.; Bauer, R.; Novalic, S.; Heisler, C. T. *Environ. Sci. Technol.* **1994**, *28*, 670.

(9) Ha, H. Y.; Anderson, M. A. *J. Environ. Eng.* **1996**, *122*, 217.

(10) Sato, S. *Langmuir* **1988**, *4*, 1156.

(11) Sampath, S.; Uchida, H.; Yoneyama, H. *J. Catal.* **1994**, *149*, 148.

(12) Haarstrick, A.; Kut, O. E.; Heinzle, E. *Environ. Sci. Technol.* **1996**, *30*, 817.

(13) Yoneyama, H.; Haga, S.; Yamanaka, S. *J. Phys. Chem.* **1989**, *93*, 4833.

(14) Tanguay, J.; Suib, S. L.; Coughlin, R. W. *J. Catal.* **1989**, *117*, 335.

(15) Liu, X.; Iu, K. K.; Thomas, J. K. *J. Chem. Soc., Faraday Trans.* **1993**, *89*, 1816.

(16) Green, K. J.; Rudham, R. J. *J. Chem. Soc., Faraday Trans.* **1993**, *89*, 1867.

(17) Fox, M. A.; Doan, K. E.; Dulay, M. T. *Res. Chem. Intermed.* **1994**, *20*, 711.

(18) Torimoto, T.; Ito, S.; Kuwabata, S.; Yoneyama, H. *Environ. Sci. Technol.* **1996**, *30*, 1275.

(19) Xu, Y.; Langford, C. H. *J. Phys. Chem.* **1995**, *99*, 11501.

(20) Minero, C.; Catozzo, F.; Pelizzetti, E. *Langmuir* **1992**, *8*, 481.

(21) Bahnemann, D.; Cunningham, J.; Fox, M. A.; Pelizzetti, E.; Pichat, P.; Serpone, N. In *Aquatic and Surface Photochemistry*; Helz, G., Zepp, R. G., Crosby, D. G. Eds.; Lewis Publisher: Boca Raton, FL, 1994; Chapter 21.

(22) Breck, D. W. *Zeolite Molecular Sieves: Structure, Chemistry and Use*; John Wiley & Sons: New York, 1971.

(23) (a) Iu, K. K.; Liu, X.; Thomas, J. K. *Mater. Res. Symp. Proc.* **1991**, *223*, 119. (b) Liu, X.; Iu, K.-K.; Thomas, J. K. *Chem. Phys. Lett.* **1992**, *195* (2,3), 163.

(24) Ramamurthy, V.; Eaton, D. F. In *The Proceedings of the 9th International Zeolite Conference, Montreal 1992*; Ballmoos, R. V., et al., Eds.; Butterworth-Heinemann: Oxford, 1993; p 587.

(25) (a) Breck, J. S.; Vartuli, J. C.; Roth, W. J.; Leonowicz, M. E.; Kresge, C. T.; Schmitt, K. D.; Chu, C. T.-W.; Olson, D. H.; Sheppard, E. W.; McCullen, S. B.; Higgins, J. B.; Schlenker, J. L. *J. Am. Chem. Soc.* **1992**, *114*, 10834. (b) Breck, J. S. U.S. Patent 5,057,296, 1991.

(26) Choi, W.; Termin, A.; Hoffmann, M. R. *J. Phys. Chem.* **1994**, *98*, 13669.

(27) Chen, C.-Y.; Li, H.-X.; Davis, M. E. *Microporous Mater.* **1993**, *2*, 17.

(28) Ryoo, R.; Kim, J. M. *J. Chem. Soc., Chem. Commun.* **1995**, 711.

(29) Corma, A.; Navarro, M. T.; Pariente, J. P. *J. Chem. Soc., Chem. Commun.* **1994**, 147. Alba, M. D.; Luan, Z.; Klinowski, J. *J. Phys. Chem.* **1996**, *100*, 2182.

(30) Yan, Z. Y.; Liu, S. Q.; Chen, T. H.; Wang, J. Z.; Li, H. X. *J. Chem. Soc., Chem. Commun.* **1995**, 973.

(31) Zhao, D.; Goldfarb, D. *J. Chem. Soc., Chem. Commun.* **1995**, 875.

(32) Reddy, K. M.; Moudrakovski, I.; Sayari, A. *J. Chem. Soc., Chem. Commun.* **1994**, 1059.

(33) Horvath, G.; Kawazoe, K. *J. Chem. Eng. Jpn.* **1983**, *16*, 470.

(34) Cullity, B. D. *Elements of X-ray Diffraction*; Addison-Wesley: Reading, MA, 1956.

(35) For example: (a) Martin, Scot T.; Morrison, C. L.; Hoffmann, M. *J. Phys. Chem.* **1994**, *98*, 13695. (b) Kormann, C.; Bahnemann, D. W.; Hoffmann, M. R. *J. Phys. Chem.* **1988**, *92*, 5196. (c) Rivera, A. P.; Tanaka, K.; Hisanaga, T. *Appl. Catal.* **1993**, *3*, 37. Tanaka, K.; Capule, M. F. V.; Hisanaga, T. *Chem. Phys. Lett.* **1991**, *187* (1,2), 73. (d) Anpo, M.; Shima, T.; Kodama, S.; Kubokawa, Y. *J. Phys. Chem.* **1987**, *91*, 4305. (e) Kato, K. *Bull. Chem. Soc. Jpn.* **1992**, *65*, 34. (d) Mills, A.; Sawunyama, P. *J. Photochem. Photobiol. A: Chem.* **1994**, *84*, 305.

(36) Hiemenz, P. C. *Principals of Colloid and Surface Chemistry*, 2nd ed.; Marcel Dekker: New York, 1986.

(37) Anderson, M. W.; Klinowski, J. *J. Chem. Soc., Faraday Trans. 1* **1986**, *82*, 3569.

(38) Mills, A.; Davies, R. *J. Photochem. Photobiol. A: Chem.* **1995**, *173*, and references therein.